Multiplexed 3D cellular super-resolution imaging with DNA-PAINT and Exchange-PAINT

Ralf Jungmann[1,2,6], Maier S Avendaño[1,2,6], Johannes B Woehrstein[1,6], Mingjie Dai[1,3], William M Shih[1,4,5] & Peng Yin[1,2]

Super-resolution fluorescence microscopy is a powerful tool for biological research, but obtaining multiplexed images for a large number of distinct target species remains challenging. Here we use the transient binding of short fluorescently labeled oligonucleotides (DNA-PAINT, a variation of point accumulation for imaging in nanoscale topography) for simple and easy-to-implement multiplexed super-resolution imaging that achieves sub-10-nm spatial resolution *in vitro* on synthetic DNA structures. We also report a multiplexing approach (Exchange-PAINT) that allows sequential imaging of multiple targets using only a single dye and a single laser source. We experimentally demonstrate ten-color super-resolution imaging *in vitro* on synthetic DNA structures as well as four-color two-dimensional (2D) imaging and three-color 3D imaging of proteins in fixed cells.

© 2014 Nature America, Inc. All rights reserved.

Far-field fluorescence microscopy has undergone major advances since the advent of methods circumventing the classical diffraction limit, i.e., super-resolution microscopy[1,2]. Most implementations 'switch' molecules between fluorescence on- and off-states to obtain subdiffraction image resolution. This switching is traditionally obtained in two ways: targeted switching actively confines the fluorescence excitation to an area smaller than the diffraction limit of light (for example, in stimulated emission depletion, or STED, microscopy[3]), whereas stochastic switching uses photoswitchable proteins or photoswitchable organic dyes (for example, in photoactivated localization microscopy (PALM)[4] and stochastic optical reconstruction microscopy (STORM)[1]). Although these methods offer unprecedented spatial resolution, they tend to be technically involved to implement, and multiplexing for a large number of distinct targets is generally challenging.

PAINT[5–7] provides an alternative stochastic super-resolution imaging method. Here imaging is carried out using diffusing fluorescent molecules that interact transiently with the sample. This method is straightforward to implement and does not require specialized equipment or conditions to obtain photoswitching, thus making it more accessible than STED or STORM for laboratories with standard instrumentation and sample-preparation capabilities. Initially, PAINT was applied to obtain super-resolved images of cell membranes[5] and artificial lipid vesicles[5]. However, a key limitation of PAINT's original formulation is that dyes interact with the sample via electrostatic coupling or hydrophobic interactions. This limits the availability of PAINT-compatible dyes, making it hard to simultaneously image specific biomolecules of interest. A recent implementation of PAINT has involved continuously and stochastically labeling specific membrane biomolecules with fluorescent ligands (such as antibodies)[6]. The approach, termed universal PAINT, achieves specific dye-sample interactions but still lacks the ability to specify interactions with programmable kinetics. Similarly to PAINT, binding of DNA intercalating dyes has also been used to obtain super-resolved images of DNA[8,9].

To achieve programmable dye interactions and to increase the specificity and the number of usable fluorophores, DNA-PAINT was developed[10]. Here stochastic switching between fluorescence on- and off-states is implemented via repetitive, transient binding of fluorescently labeled oligonucleotides ('imager' strands) to complementary 'docking' strands on DNA nanostructures (**Fig. 1a**,**b**). In the unbound state, only background fluorescence from partially quenched[10] imager strands is observed (**Fig. 1a**). However, upon binding and immobilization of an imager strand, fluorescence emission is detected using total-internal-reflection (TIR) or highly inclined and laminated optical sheet (HILO) microscopy[11]. DNA-PAINT enhances PAINT's simplicity and ease of use with the programmability and specificity of DNA hybridization. Notably, it enables a wide range of fluorescence on- and off-times; these can be adjusted by tuning the binding strength and concentration of the imager strand[10]. DNA-PAINT has been used to obtain multicolor subdiffraction images of DNA nanostructures[10,12–15] with ~25-nm spatial resolution[14]. Spectral multiplexing is straightforward as no external photoswitching of dyes is necessary, and imaging specificity is obtained through orthogonality of DNA sequences coupled to spectrally distinct dyes[13].

By linking DNA-PAINT docking strands to antibodies, we have extended the DNA-PAINT method to enable multiplexed 2D and

[1]Wyss Institute for Biologically Inspired Engineering, Harvard University, Boston, Massachusetts, USA. [2]Department of Systems Biology, Harvard Medical School, Boston, Massachusetts, USA. [3]Program in Biophysics, Harvard University, Cambridge, Massachusetts, USA. [4]Department of Biological Chemistry and Molecular Pharmacology, Harvard Medical School, Boston, Massachusetts, USA. [5]Department of Cancer Biology, Dana-Farber Cancer Institute, Boston, Massachusetts, USA. [6]These authors contributed equally to this work. Correspondence should be addressed to P.Y. (py@hms.harvard.edu).

RECEIVED 1 AUGUST 2013; ACCEPTED 3 JANUARY 2014; PUBLISHED ONLINE 2 FEBRUARY 2014; DOI:10.1038/NMETH.2835

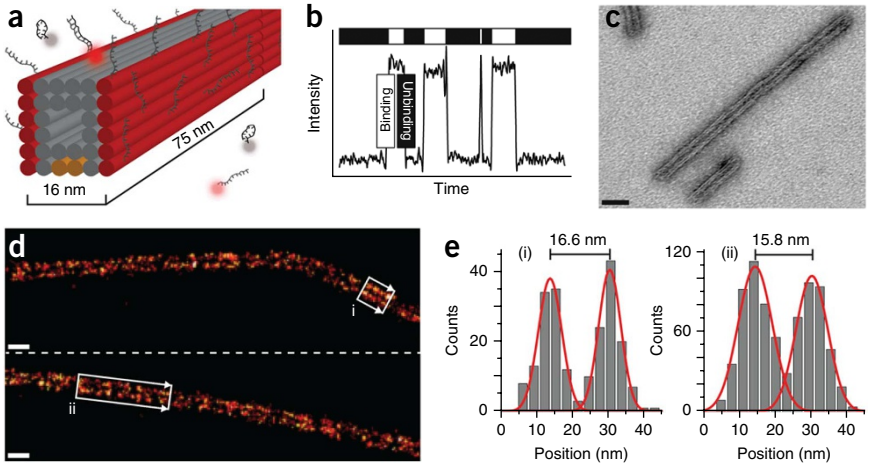


Figure 1 | DNA-PAINT. (**a**) A microtubule-like DNA origami polymer (cylinders represent DNA double helices) is decorated with single-stranded extensions (docking strands) on two opposite faces (red) spaced ~16 nm apart. Complementary fluorescent imager strands transiently bind from solution to docking strands. Biotinylated strands (present on orange helices) immobilize the structures to glass surfaces for fluorescence imaging. (**b**) Transient binding between imager and docking strands produces fluorescence blinking, allowing stochastic super-resolution imaging. (**c**) Transmission electron microscopy image of origami polymers with a measured width of 16 ± 1 nm (mean ± s.d.). (**d**) DNA-PAINT super-resolution images obtained using Cy3b-labeled imager strands (15,000 frames, 5-Hz frame rate). Two distinct lines are visible. (**e**) Cross-sectional histograms of the boxed areas i and ii in **d** (arrows denote histogram direction) both reveal a distance of ~16 nm as designed (FWHM of each distribution is ~7–10 nm). Scale bars, 40 nm.

© 2014 Nature America, Inc. All rights reserved.

3D super-resolution imaging of protein components in fixed cells. We report sub-10-nm lateral imaging resolution *in vitro* of synthetic DNA structures without the use of a sophisticated setup (in contrast with STED[3] or dual-objective STORM[16]) or specialized experimental conditions such as dye-caging approaches[17]. We used the unique programmability of DNA molecules to perform sequential multiplexing (with Exchange-PAINT) using only a single fluorescent dye and obtained the first ten-color *in vitro* super-resolution image on DNA nanostructures. We also show the applicability of Exchange-PAINT to cellular imaging by demonstrating four-color imaging of protein targets in fixed cells and three-color 3D imaging.

RESULTS

Sub-10-nm *in vitro* imaging with DNA-PAINT

First we optimized the spatial resolution of DNA-PAINT relative to that of earlier DNA-PAINT studies[10,13–15] through enhanced drift correction and higher localization accuracy. We achieved the latter by collecting more emitted photons per binding event through optimization of fluorescence on-times and camera integration time and by increasing laser excitation intensities. Extracting more photons per binding event was also facilitated by the fact that DNA-PAINT imaging is not prone to photobleaching, as imager strands are continuously replenished from solution[10]. This replenishing also allows nearly 100% imaging efficiency of all docking sites[10]. This imaging efficiency of docking sites does not necessarily translate to imaging efficiency of targets, as the labeling efficiency of targets with docking strands may not be 100%. However, if present and accessible, every docking site should eventually be imaged during data acquisition[10].

We evaluated imaging performance by visualizing DNA origami structures that mimic *in vitro*–assembled microtubules (**Fig. 1a**). In DNA origami, a long ssDNA molecule (the 'scaffold') is 'folded' into a desired shape or pattern by the sequence-specific binding of hundreds of short oligonucleotides (the 'staple' strands) to designated regions on the scaffold[18,19] (**Supplementary Fig. 1**). The DNA origami monomer is a tunnel-like structure (with dimensions of ~16 nm × ~16 nm × ~75 nm). We linked monomers using connector strands to form a homopolymer mimicking microtubules (**Fig. 1c**), which formed with high yield (**Supplementary Fig. 2**). To allow for DNA-PAINT imaging, we extended staple strands on two opposite faces of the structure by adding single-stranded docking sites at the 3′ end. We bound assembled polymers to a BSA-biotin-streptavidin glass surface using biotinylated staple strands extruding from the bottom of the structure[10,13,14,20]. DNA-PAINT was then performed using Cy3b-labeled imager strands.

The super-resolved image revealed two adjacent lines spaced ~16 nm apart, a geometry matching that of the designed microtubule-like origami (**Fig. 1d**). The cross-sectional profiles of two regions of interest possessed well-separated peaks at the designed distance with a full width at half maximum (FWHM) of ~7–10 nm (**Fig. 1e** and **Supplementary Fig. 3**). We note that this resolution was obtained in standard DNA hybridization buffer without the use of oxygen scavengers[21], triplet-state quenchers[22] or redox systems[23].

Straightforward extension to multicolor imaging was obtained by coupling spectrally distinct dyes to orthogonal imager strand sequences as reported previously[13] (**Supplementary Fig. 4**). The orthogonality of the imager strand sequences prevents cross-talk between different color channels (**Supplementary Fig. 4b–d**).

Multiplexed cellular imaging with DNA-PAINT

To image cellular components with DNA-PAINT, we specifically labeled protein targets using antibodies conjugated with DNA docking strands (**Fig. 2**). We formed the conjugates by first reacting biotinylated docking strands with streptavidin and then incubating with biotinylated antibodies. We first immunostained fixed HeLa cells using a preassembled antibody-DNA conjugate against β-tubulin. Atto 655–labeled imager strands were then introduced, and imaging was performed using HILO microscopy[11]. The resulting super-resolution images showed a clear increase in spatial resolution over that of the diffraction-limited representation (**Fig. 2a–c**). A cross-sectional profile yielded a distance of ~79 nm between two adjacent microtubules with an apparent width of ~47 and ~44 nm for each (**Supplementary Fig. 5**), dimensions consistent with those in earlier reports[24]. We observed little to no nonspecific binding of imager strands to nonlabeled cellular components (see below for quantitative characterization and discussion of nonspecific binding).

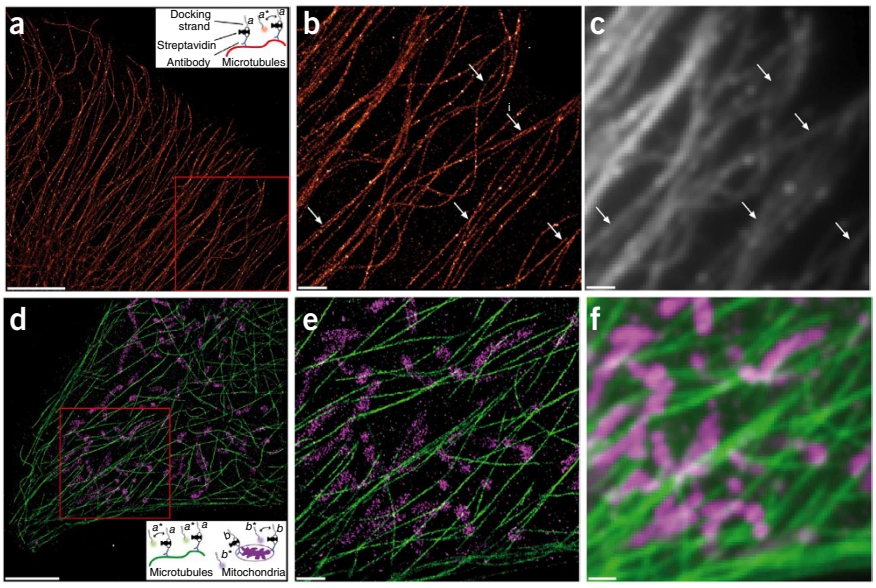


Figure 2 | Spectrally multiplexed DNA-PAINT super-resolution imaging of microtubules and mitochondria inside fixed cells. (**a**) DNA-PAINT super-resolution image of microtubules inside a fixed HeLa cell using Atto 655–labeled imager strands (10,000 frames, 10-Hz frame rate). Inset, labeling and imaging schematic for DNA-PAINT in a cellular environment. Microtubules are labeled with a preassembled antibody-DNA conjugate, which is formed between a biotinylated anti-tubulin antibody and a biotinylated DNA docking strand (*a*) using a streptavidin bridge. *a** indicates the complementary imager strand. (**b**) Zoomed-in view of the boxed area in **a**. (**c**) Diffraction-limited representation of the area in **b**. Arrows in **b** and **c** highlight positions where the increase in resolution of the DNA-PAINT image is clearly visible. Adjacent microtubules with an apparent width of ~46 nm at position i are separated by ~79 nm (see also **Supplementary Fig. 5**). (**d**) Dual-color DNA-PAINT super-resolution image (15,000 frames, 10-Hz frame rate) of microtubules and mitochondria inside a fixed HeLa cell obtained using Cy3b-labeled imager strands (*a**) for microtubules (green) and orthogonal Atto 655–labeled imager strands (*b**) for mitochondria (purple). Inset, labeling and imaging schematic. (**e**) Zoomed-in view of the boxed area in **d**. (**f**) Diffraction-limited image of the area in **e**. Scale bars, 5 µm (**a**,**d**) and 1 µm (**b**,**c**,**e**,**f**).

© 2014 Nature America, Inc. All rights reserved.

We achieved multicolor imaging by using orthogonal imager strands coupled to spectrally distinct dyes. We labeled microtubules in a fixed HeLa cell with a preassembled antibody-DNA conjugate carrying a docking sequence for Cy3b-labeled imager strands, and we stained mitochondria using a second antibody linked to an orthogonal sequence for Atto 655–labeled imager strands (**Fig. 2d**). Although Cy3b– and Atto 655–labeled imager strands coexisted in solution, imaging was performed sequentially. Images were drift corrected, and we aligned different color channels using gold nanoparticles as fiducial markers (Online Methods). The resulting super-resolution images showed a clear increase in spatial resolution as compared to the diffraction-limited representation, and no cross-talk between colors was observed (**Fig. 2d**–**f**).

Ten-color super-resolution imaging with Exchange-PAINT

As imager strands only transiently bind to the docking strands, DNA-PAINT allows for a new multiplexing approach wherein orthogonal imager strands are sequentially applied to the same sample. This approach, which we call Exchange-PAINT, is depicted in **Figure 3a**. Initially, different target species are labeled with orthogonal docking strands. Once all components are labeled, the first imager strand species P1* (complementary to docking strands P1) is introduced and a DNA-PAINT image is acquired only for the targets labeled with P1. In a subsequent washing step, imager strands P1* are removed and imager strands P2* are introduced. Another image for only P2 is then acquired. In each imaging step, the respective docking sites are super-resolved and a unique pseudocolor is assigned. Washing and imaging steps are repeated until all desired targets are imaged. These images are then aligned and combined to produce the final multicolor image for the entire sample.

In contrast with the spectral multiplexing approach described in the previous section, in Exchange-PAINT, the same dye—and, hence, the same laser—is used for all the target species. As such, multiplexing is limited only by the number of possible orthogonal DNA docking sequences instead of the number of spectrally distinct dyes (a typical limit for most previous fluorescence imaging methods).

To demonstrate ten-color super-resolution imaging of DNA structures using Exchange-PAINT, we designed ten unique rectangular DNA origami shapes[18], each displaying a distinct pattern of orthogonal docking strands that resembles a digit between 0 and 9 (**Fig. 3b**). After surface immobilization of all ten structures, we performed sequential imaging using a custom-made fluidic chamber (**Supplementary Fig. 6a**) for easy liquid handling. Ten orthogonal imager strands (P1* to P10*), all labeled with Cy3b, were used to perform Exchange-PAINT. The resulting digits from all ten imaging rounds are shown in **Figure 3c**. Each target was resolved with high spatial resolution. Cross-sectional histograms along the bars of the digits showed sub-10-nm FWHM of the distributions (data not shown). Note that high resolution was maintained for all digits, as the same optimized dye (Cy3b) and imaging conditions were used in each cycle.

A combined image of all ten rounds (**Fig. 3d** and **Supplementary Fig. 7**) demonstrates specific interaction of imager strands with respective targets with no observable cross-talk between cycles. An apparent green digit 5 instead of 2 was observed (**Fig. 3d**). This is likely not a falsely imaged digit 5 from cross-talk but rather a mirrored digit 2 (**Supplementary Fig. 8**). A mirrored image likely results from an origami immobilized upside down[25], with docking strands trapped underneath yet still accessible to imager strands.

The fluidic setup is designed to minimize sample movement by decoupling the fluid reservoir and syringe from the actual flow chamber via flexible tubing. To avoid sample distortion, we took special care to ensure gentle fluid flow during washing steps. To verify that the sample indeed exhibited little movement and little to no distortion, we performed a ten-round Exchange-PAINT experiment. We imaged the DNA origami for digit 4 in the first round and reimaged it after ten rounds of buffer exchange. The total sample movement (physical movement of the fluidic

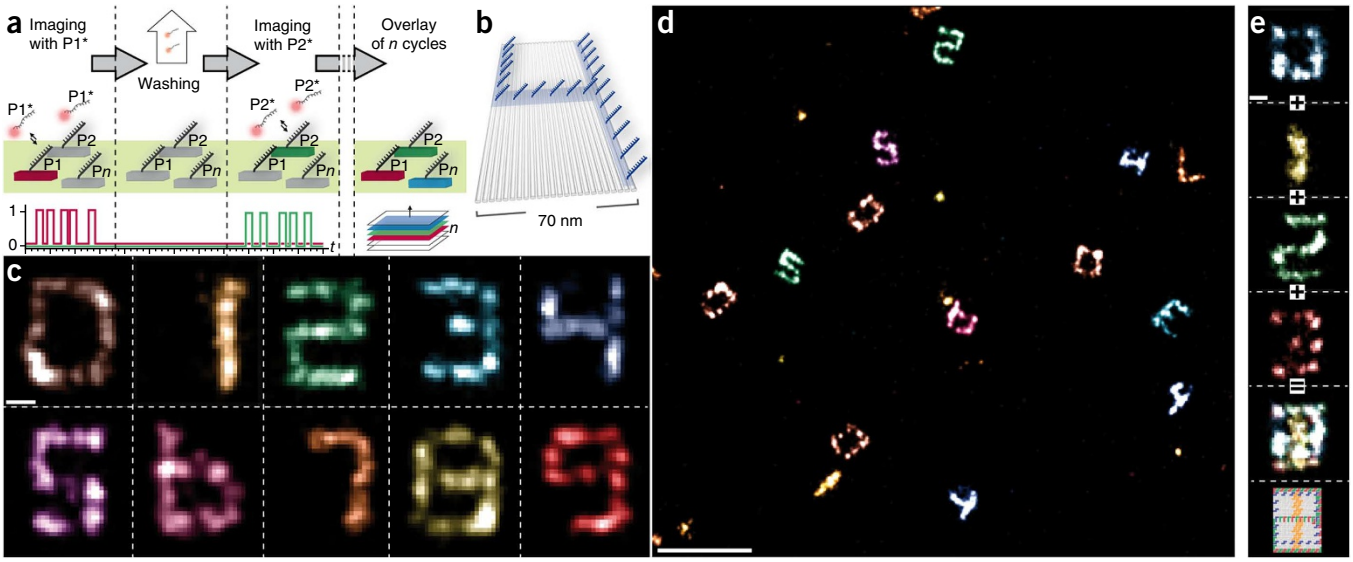


Figure 3 | Exchange-PAINT. (**a**) Exchange-PAINT schematic showing sequential imaging of multiple targets using imager strands labeled with the same fluorophore. (**b**) Schematic of a DNA origami pattern (70 nm × 100 nm) displaying docking strands that resemble the digit "4." (**c**) Pseudocolor images of ten different origami structures displaying digits 0–9 in one sample with high resolution (FWHM of bar-like features <10 nm) and specificity. The images were obtained using only one fluorophore (Cy3b) through ten imaging-washing cycles (imaging: 7,500 frames per cycle, 5-Hz frame rate; washing: 1–2 min per cycle). (**d**) Combined overview image of all ten Exchange-PAINT cycles, demonstrating specific interaction with the respective target with no cross-talk between imaging cycles. (**e**) Four-color image of digits 0–3 that are all present on the same DNA origami (10,000 frames each, 5-Hz frame rate; schematic at the bottom). Scale bars, 25 nm (**c**,**e**) and 250 nm (**d**).

© 2014 Nature America, Inc. All rights reserved.

chamber with respect to the objective) was less than 2 µm, which could easily be corrected using fiducial markers. Normalized cross-correlation analysis for select structures produced a correlation coefficient of 0.92 (**Supplementary Fig. 9**), a result indicative of almost no sample distortion (see also the Discussion below).

Finally, using Exchange-PAINT, we successfully imaged four different digit patterns on the same DNA origami structure (**Fig. 3e** and **Supplementary Fig. 10**). Thus, Exchange-PAINT is not limited to spatially separate species and can resolve subdiffraction patterns on the same structure with no observable cross-talk or sample distortion. Aligning images from different Exchange-PAINT rounds is straightforward using DNA origami-based drift markers. Additionally, because imaging is performed using the same dye, no chromatic aberration needs to be corrected between imaging rounds.

Multiplexed cellular imaging with Exchange-PAINT

We next demonstrated multiplexed *in situ* imaging in a fixed HeLa cell with Exchange-PAINT. **Figure 4a** shows four-color super-resolution images obtained by sequential imaging using only a single dye (Atto 655). Using custom-made fluidic chambers (**Supplementary Fig. 6b**), we obtained super-resolution images of β-tubulin in microtubules, COX IV in mitochondria, TGN46 in the Golgi complex and PMP70 in peroxisomes. Imaging and washing was performed in a similar fashion as for DNA structures. Again, we saw little to no nonspecific binding of the imager strands to nonlabeled components (**Supplementary Fig. 11**).

To quantify possible nonspecific interactions of the imager strands with cellular components, we performed Exchange-PAINT experiments in which no DNA-PAINT docking strands were present on the antibody-streptavidin conjugates, but otherwise we performed the labeling and imaging process as described above (**Supplementary Fig. 12**). We observed minimal nonspecific interaction of the imager strands (Atto 655 or Cy3b) with the cellular components including genomic DNA. Nonspecific interactions can be excluded by analyzing their blinking behavior in an intensity-versus-time trace[13]: such interactions lead to nonrepeating localization events and therefore show an easily identifiable blinking signature (a non-exponential distribution of on- and off-times) that differs from that of specific DNA hybridization interactions (**Supplementary Fig. 12**).

To quantify potential sample distortion in cellular Exchange-PAINT imaging, we performed a study similar to that for the *in vitro* case. Here we imaged microtubules and mitochondria in four rounds of Exchange-PAINT by imaging microtubules first and then mitochondria and then repeating the process. We then selected a region of interest in each image and performed a normalized cross-correlation analysis. We obtained cross-correlation coefficients of 0.80 and 0.96 for the microtubule and mitochondria images, respectively (**Supplementary Fig. 13**), values indicative of minimal sample distortion.

We note that, even in a super-resolution image without liquid exchange, one cannot expect 100% correlation between two consecutive images of the same region in a sample owing to the stochastic nature of the image formation. To see this effect, one can simply split a super-resolution raw data set into two parts of equal length, perform a stochastic reconstruction and calculate the normalized cross-correlation coefficient for these two supposedly equal images. We performed this analysis for a subregion of the microtubule image in **Figure 4b** and obtained a coefficient of 0.88, similar to the Exchange-PAINT case of 0.80 (**Supplementary Fig. 13**).

Finally, we used optical astigmatism imaging[26,27] to demonstrate 3D Exchange-PAINT super-resolution imaging in a fixed HeLa cell. We labeled microtubules, mitochondria and peroxisomes and obtained three-color 3D super-resolution Exchange-PAINT

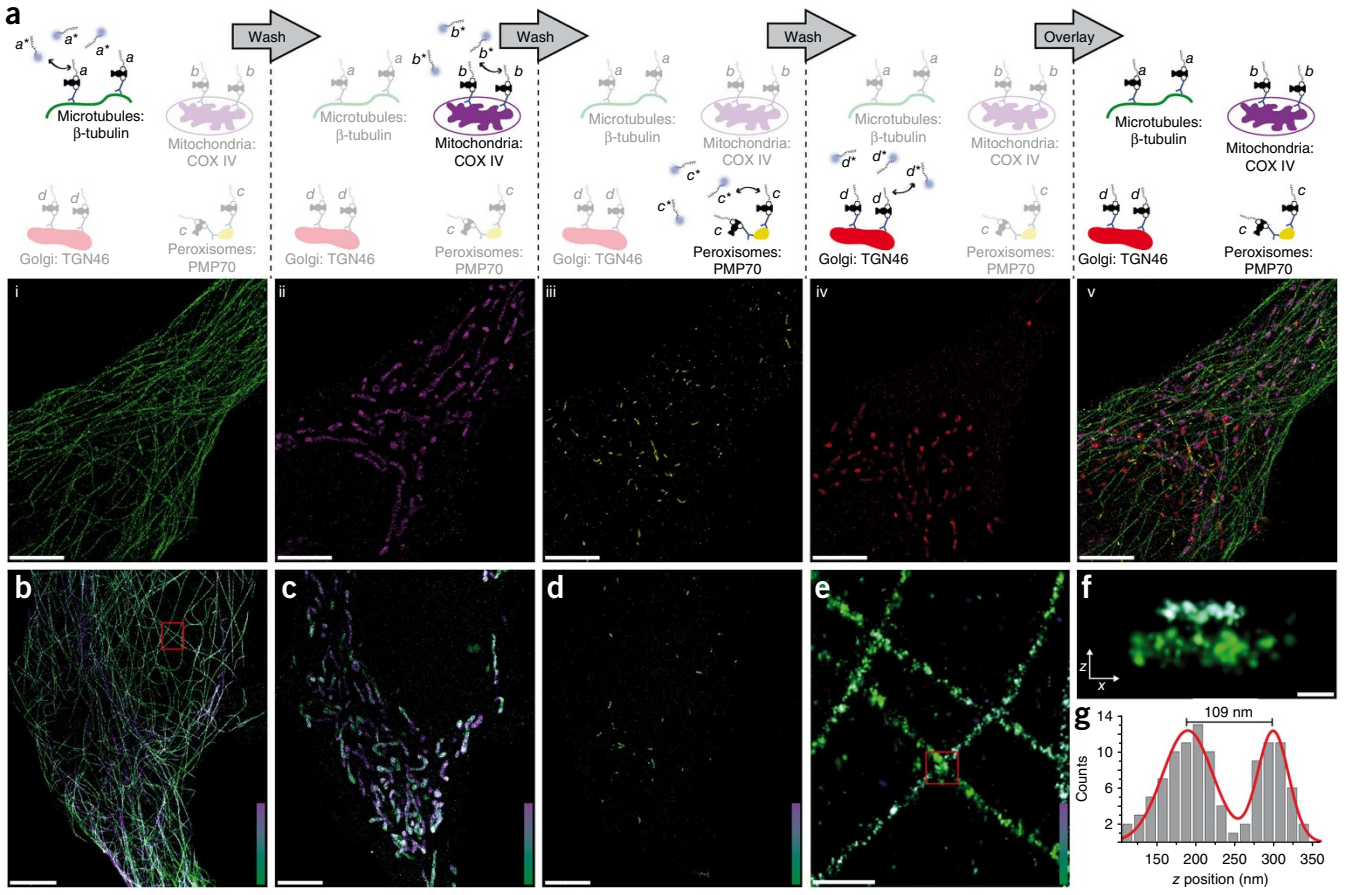


Figure 4 | Multiplexed 2D and 3D Exchange-PAINT super-resolution imaging in fixed cells. Each target is labeled with an antibody carrying a unique DNA-PAINT docking sequence. 2D and 3D imaging are performed using imager strands labeled with Atto 655 and Cy3b, respectively. (**a**, **i**) Only imager strands *a** are present, and microtubules are specifically imaged. (**a**, **ii**) After imager strands *a** are washed out, imager strands *b** are introduced and COX IV proteins in mitochondria are imaged. TGN46 proteins in the Golgi complex (**a**, **iii**) and PMP70 proteins in peroxisomes (**a**, **iv**) are imaged in the same way (imaging: 15,000 frames per cycle, 10-Hz imaging rate; washing: 1–2 min per cycle). (**a**, **v**) Overlay of all four targets. (**b**–**g**) Three-color 3D Exchange-PAINT images using Cy3b-labeled imager strands. (**b**) 3D image of microtubules; color indicates height on a scale from 0 nm (green) to 800 nm (purple). (**c**) 3D image of mitochondria; the height scale is 40–1,100 nm. (**d**) 3D image of peroxisomes; the height scale is 0–700 nm. (**e**) Zoomed-in view of the boxed area in **b**; the height scale is 0–700 nm. (**f**) *xz* profile of the boxed area in **e**. (**g**) A two-component Gaussian fit reveals a distance of ~109 nm in *z* of two adjacent microtubules. For 3D imaging: 50,000 frames per cycle, 16-Hz imaging rate; washing: 1–2 min per cycle. Scale bars: 5 µm (**a**–**d**), 500 nm (**e**) and 100 nm (**f**).

images using Cy3b (**Fig. 4b–d** and **Supplementary Fig. 14**). A magnified image revealed separate microtubules crossing each other in different *z* planes (**Fig. 4e**,**f**). A cross-sectional histogram in *z* yielded a distance of ~109 nm, which is well below the diffraction limit (**Fig. 4g**).

DISCUSSION

Sequential multiplexing, as that achieved with Exchange-PAINT, provides a complementary approach to previous spectral and geometric multiplexing[13,28]. Compared to geometric multiplexing[13,28], Exchange-PAINT uses a more compact labeling entity (an ~9-nt DNA strand), but this should allow up to several hundred noninteracting sequences within tight bounds for dissociation kinetics. Exchange-PAINT may enable a substantial increase in multiplexing for both super-resolution and diffraction-limited imaging. In contrast with spectral multiplexing[28,29], Exchange-PAINT uses only a single fluorophore, thereby allowing the selection of an optimal dye with respect to its photophysical properties (such as the number of emittable photons) for super-resolution imaging. Unlike previous multiplexing approaches for diffraction-limited imaging based on DNA strand exchange reactions[30] and *in situ* sequencing[31], Exchange-PAINT does not involve labeling and erasing steps, as imager strands bind to docking strands only transiently. Exchange-PAINT thus permits simpler experimental procedures and faster image acquisition (~1–2 min of washing between imaging cycles) while preserving the intrinsic super-resolution capability of DNA-PAINT.

Fully translating the *in vitro* imaging capability of DNA-PAINT and Exchange-PAINT to *in situ* imaging of cellular components will benefit from strategies to label diverse cellular targets with high specificity and efficiency. One way to facilitate this goal, as noted by other researchers[17,24,32], is reducing the label size. Our current antibody-DNA conjugation method based on streptavidin bridging, though providing a simple and modular approach, results in a rather bulky conjugate with large linker distances that preclude obtaining the sub-10-nm resolution we demonstrated by direct labeling of DNA nanostructures with imager strands. Thus a next logical step would be direct coupling of primary

© 2014 Nature America, Inc. All rights reserved.

antibodies to DNA strands[33] without a streptavidin intermediate. Additionally, to further decrease the label size, it would be advantageous to use nanobody- or aptamer-based labeling strategies[24,32], with the latter serving as a natural extension to DNA-PAINT imaging as it already uses nucleic acid–based interactions. In addition to its use in protein imaging, our method should be directly applicable to DNA and RNA imaging in fixed cells: for example, by using FISH methods[28,34].

DNA-PAINT and Exchange-PAINT provide a simple and robust method for highly multiplexed super-resolution imaging. With further development, we anticipate it will become a useful and standard tool for studying complex biomolecular systems.

METHODS

Methods and any associated references are available in the online version of the paper.

Note: Any Supplementary Information and Source Data files are available in the online version of the paper.

ACKNOWLEDGMENTS

We thank J. Nicoludis and M.T. Strauss for help with DNA origami design, T. Schlichthaerle for transmission electron microscopy imaging support and M. Zhang for help with DLD1 cells. We thank C. Steinhauer for help with DNA-PAINT software development and fruitful discussions. We thank R.D. Barish for critical reading and commenting on the manuscript. This work is supported by a US National Institutes of Health (NIH) Director's New Innovator Award (1DP2OD007292), an NIH Transformative Research Award (1R01EB018659), an NIH grant (5R21HD072481), an Office of Naval Research (ONR) Young Investigator Program Award (N000141110914), ONR grants (N000141010827 and N000141310593), a US National Science Foundation (NSF) Faculty Early Career Development Award (CCF1054898), an NSF grant (CCF1162459) and a Wyss Institute for Biologically Engineering Faculty Startup Fund to P.Y., and an NIH Director's New Innovator Award (1DP2OD004641) and a Wyss Institute for Biologically Inspired Engineering Faculty Award to W.M.S. R.J. acknowledges support from the Alexander von Humboldt-Foundation through a Feodor-Lynen Fellowship. M.S.A. and M.D. acknowledge support from Howard Hughes Medical Institute International Student Research Fellowships.

AUTHOR CONTRIBUTIONS

R.J., M.S.A. and J.B.W. contributed equally to this work. R.J. and M.S.A. conceived of the study, designed and performed the experiments, analyzed the data and wrote the manuscript. J.B.W. designed and performed the experiments, analyzed the data and wrote the manuscript. M.D. performed the experiments, analyzed the data and developed the drift correction software. W.M.S. supervised the project, discussed the results and critiqued the paper. P.Y. conceived of, designed and supervised the study, interpreted the data and wrote the manuscript. All authors reviewed and approved the manuscript.

COMPETING FINANCIAL INTERESTS

The authors declare competing financial interests: details are available in the online version of the paper.

Reprints and permissions information is available online at http://www.nature.com/reprints/index.html.

1. Rust, M.J., Bates, M. & Zhuang, X. Sub-diffraction-limit imaging by stochastic optical reconstruction microscopy (STORM). *Nat. Methods* **3**, 793–795 (2006).
2. Hell, S.W. Microscopy and its focal switch. *Nat. Methods* **6**, 24–32 (2009).
3. Hell, S.W. & Wichmann, J. Breaking the diffraction resolution limit by stimulated emission: stimulated-emission-depletion fluorescence microscopy. *Opt. Lett.* **19**, 780–782 (1994).
4. Betzig, E. *et al.* Imaging intracellular fluorescent proteins at nanometer resolution. *Science* **313**, 1642–1645 (2006).
5. Sharonov, A. & Hochstrasser, R.M. Wide-field subdiffraction imaging by accumulated binding of diffusing probes. *Proc. Natl. Acad. Sci. USA* **103**, 18911–18916 (2006).
6. Giannone, G. *et al.* Dynamic superresolution imaging of endogenous proteins on living cells at ultra-high density. *Biophys. J.* **99**, 1303–1310 (2010).
7. Lew, M.D. *et al.* Three-dimensional superresolution colocalization of intracellular protein superstructures and the cell surface in live *Caulobacter crescentus*. *Proc. Natl. Acad. Sci. USA* **108**, E1102–E1110 (2011).
8. Flors, C., Ravarani, C.N. & Dryden, D.T. Super-resolution imaging of DNA labelled with intercalating dyes. *ChemPhysChem* **10**, 2201–2204 (2009).
9. Schoen, I., Ries, J., Klotzsch, E., Ewers, H. & Vogel, V. Binding-activated localization microscopy of DNA structures. *Nano Lett.* **11**, 4008–4011 (2011).
10. Jungmann, R. *et al.* Single-molecule kinetics and super-resolution microscopy by fluorescence imaging of transient binding on DNA origami. *Nano Lett.* **10**, 4756–4761 (2010).
11. Tokunaga, M., Imamoto, N. & Sakata-Sogawa, K. Highly inclined thin illumination enables clear single-molecule imaging in cells. *Nat. Methods* **5**, 159–161 (2008).
12. Jungmann, R., Scheible, M. & Simmel, F.C. Nanoscale imaging in DNA nanotechnology. *Wiley Interdiscip. Rev. Nanomed. Nanobiotechnol.* **4**, 66–81 (2012).
13. Lin, C. *et al.* Submicrometre geometrically encoded fluorescent barcodes self-assembled from DNA. *Nat. Chem.* **4**, 832–839 (2012).
14. Derr, N.D. *et al.* Tug-of-war in motor protein ensembles revealed with a programmable DNA origami scaffold. *Science* **338**, 662–665 (2012).
15. Johnson-Buck, A. *et al.* Super-resolution fingerprinting detects chemical reactions and idiosyncrasies of single DNA pegboards. *Nano Lett.* **13**, 728–733 (2013).
16. Xu, K., Babcock, H.P. & Zhuang, X. Dual-objective STORM reveals three-dimensional filament organization in the actin cytoskeleton. *Nat. Methods* **9**, 185–188 (2012).
17. Vaughan, J.C., Jia, S. & Zhuang, X. Ultrabright photoactivatable fluorophores created by reductive caging. *Nat. Methods* **9**, 1181–1184 (2012).
18. Rothemund, P.W. Folding DNA to create nanoscale shapes and patterns. *Nature* **440**, 297–302 (2006).
19. Douglas, S.M. *et al.* Self-assembly of DNA into nanoscale three-dimensional shapes. *Nature* **459**, 414–418 (2009).
20. Steinhauer, C., Jungmann, R., Sobey, T.L., Simmel, F.C. & Tinnefeld, P. DNA origami as a nanoscopic ruler for super-resolution microscopy. *Angew. Chem. Int. Ed. Engl.* **48**, 8870–8873 (2009).
21. Aitken, C.E., Marshall, R.A. & Puglisi, J.D. An oxygen scavenging system for improvement of dye stability in single-molecule fluorescence experiments. *Biophys. J.* **94**, 1826–1835 (2008).
22. Rasnik, I., McKinney, S.A. & Ha, T. Nonblinking and long-lasting single-molecule fluorescence imaging. *Nat. Methods* **3**, 891–893 (2006).
23. Vogelsang, J. *et al.* A reducing and oxidizing system minimizes photobleaching and blinking of fluorescent dyes. *Angew. Chem. Int. Ed. Engl.* **47**, 5465–5469 (2008).
24. Ries, J., Kaplan, C., Platonova, E., Eghlidi, H. & Ewers, H. A simple, versatile method for GFP-based super-resolution microscopy via nanobodies. *Nat. Methods* **9**, 582–584 (2012).
25. Wu, N. *et al.* Molecular threading and tunable molecular recognition on DNA origami nanostructures. *J. Am. Chem. Soc.* **135**, 12172–12175 (2013).
26. Kao, H.P. & Verkman, A.S. Tracking of single fluorescent particles in three dimensions: use of cylindrical optics to encode particle position. *Biophys. J.* **67**, 1291–1300 (1994).
27. Huang, B., Wang, W., Bates, M. & Zhuang, X. Three-dimensional super-resolution imaging by stochastic optical reconstruction microscopy. *Science* **319**, 810–813 (2008).
28. Lubeck, E. & Cai, L. Single-cell systems biology by super-resolution imaging and combinatorial labeling. *Nat. Methods* **9**, 743–748 (2012).
29. Bates, M., Dempsey, G.T., Chen, K.H. & Zhuang, X. Multicolor super-resolution fluorescence imaging via multi-parameter fluorophore detection. *ChemPhysChem* **13**, 99–107 (2012).
30. Schweller, R.M. *et al.* Multiplexed *in situ* immunofluorescence using dynamic DNA complexes. *Angew. Chem. Int. Ed. Engl.* **51**, 9292–9296 (2012).
31. Ke, R. *et al.* *In situ* sequencing for RNA analysis in preserved tissue and cells. *Nat. Methods* **10**, 857–860 (2013).
32. Opazo, F. *et al.* Aptamers as potential tools for super-resolution microscopy. *Nat. Methods* **9**, 938–939 (2012).
33. Kazane, S.A. *et al.* Site-specific DNA-antibody conjugates for specific and sensitive immuno-PCR. *Proc. Natl. Acad. Sci. USA* **109**, 3731–3736 (2012).
34. Beliveau, B.J. *et al.* Versatile design and synthesis platform for visualizing genomes with Oligopaint FISH probes. *Proc. Natl. Acad. Sci. USA* **109**, 21301–21306 (2012).

© 2014 Nature America, Inc. All rights reserved.

ONLINE METHODS

Materials. Unmodified DNA oligonucleotides were purchased from Integrated DNA Technologies. Fluorescently modified DNA oligonucleotides were purchased from Biosynthesis. Biotinylated monoclonal antibodies against β-tubulin (9F3; catalog number: 6181) and COX IV (3E11; catalog number: 6014) were purchased from Cell Signaling. Anti-PMP70 (catalog number: ab28499) was purchased from Abcam. Anti-TGN46 (catalog number: NBP1-49643B) was purchased from VWR. Streptavidin was purchased from Invitrogen (catalog number: S-888). Bovine serum albumin (BSA) and BSA-biotin obtained from Sigma-Aldrich (catalog number: A8549). Glass slides and coverslips were purchased from VWR. Lab-Tek II chambered coverglass was purchased from Thermo Fisher Scientific. M13mp18 scaffold was obtained from New England BioLabs. p8064 scaffold for microtubule-like DNA origami structures was prepared as described before[19]. Freeze 'N Squeeze columns were ordered from Bio-Rad. TetraSpeck Beads were purchased from Life Technologies. Paraformaldehyde, glutaraldehyde and TEM grids (FORMVAR 400 mesh copper grids) were obtained from Electron Microscopy Sciences.

Three buffers were used for sample preparation and imaging: buffer A (10 mM Tris-HCl, 100 mM NaCl, 0.05% Tween 20, pH 7.5), buffer B (5 mM Tris-HCl, 10 mM $MgCl_2$, 1 mM EDTA, 0.05% Tween 20, pH 8) and buffer C (1× PBS, 500 mM NaCl, pH 8).

Optical setup. Fluorescence imaging was carried out on an inverted Nikon Eclipse Ti microscope (Nikon Instruments) with the Perfect Focus System, applying an objective-type TIRF configuration using a Nikon TIRF illuminator with an oil-immersion objective (CFI Apo TIRF 100×, numerical aperture (NA) 1.49, oil). For 2D imaging an additional 1.5× magnification was used to obtain a final magnification of ~150-fold, corresponding to a pixel size of 107 nm. Three lasers were used for excitation: 488 nm (200 mW nominal, Coherent Sapphire), 561 nm (200 mW nominal, Coherent Sapphire) and 647 nm (300 mW nominal, MBP Communications). The laser beam was passed through cleanup filters (ZT488/10, ZET561/10 and ZET640/20, Chroma Technology) and coupled into the microscope objective using a multiband beam splitter (ZT488rdc/ZT561rdc/ZT640rdc, Chroma Technology). Fluorescence light was spectrally filtered with emission filters (ET525/50m, ET600/50m and ET700/75m, Chroma Technology) and imaged on an electron-multiplying charge-coupled device (EMCCD) camera (iXon X3 DU-897, Andor Technologies).

DNA origami self-assembly. The microtubule-like DNA origami structures were formed in a one-pot reaction with a 40-µl total volume containing 10 nM scaffold strand (p8064), 500 nM folding staples and biotin handles, 750 nM biotin anti-handles and 1.1 µM DNA-PAINT docking strands in folding buffer (1× TAE buffer with 20 mM $MgCl_2$). The solution was annealed using a thermal ramp[13] cooling from 80 °C to 14 °C over the course of 15 h. After self-assembly, monomeric structures were purified by agarose gel electrophoresis (1.5% agarose, 0.5× TBE, 10 mM $MgCl_2$, 1× SybrSafe) at 4.5 V/cm for 1.5 h (see **Supplementary Fig. 2**). Gel bands were cut, crushed and filled into a Freeze 'N Squeeze column and spun for 5 min at 1,000*g* at 4 °C. Polymerization was carried out at 30 °C for 48 h with a fivefold excess of polymerization staples in folding buffer. Polymerized structures were used for imaging without further purification.

DNA origami drift markers were self-assembled in a one-pot reaction (40-µl total volume, 20 nM M13mp18 scaffold, 100 nM biotinylated staples, 530 nM staples with DNA-PAINT docking sites, 1× TAE with 12.5 mM $MgCl_2$). Self-assembled structures were purified as described before.

DNA origami structures for the four-color *in vitro* Exchange-PAINT demonstration were self-assembled in a one-pot reaction (40-µl total volume, 30 nM M13mp18 scaffold, 470 nM biotinylated staples, 400 nM staples with docking sites for number imaging, 370 nM core structure staples, 1× TAE with 12.5 mM $MgCl_2$). Self-assembled structures were purified as described before.

DNA origami structures for the ten-color *in vitro* Exchange-PAINT demonstration were self-assembled in a one-pot reaction (40-µl total volume, 30 nM M13mp18 scaffold, 36 nM biotinylated staples, 750 nM staples with docking sites for number imaging, 300 nM core structure staples, 1× TAE with 12.5 mM $MgCl_2$). Structures were not purified. Excessive staples were washed out of the sample after immobilization of the structure on the surface.

DNA strand sequences for the microtubule-like DNA origami structures can be found in **Supplementary Table 1**. DNA strand sequences for DNA origami drift markers can be found in **Supplementary Table 2**. DNA strand sequences for DNA origami structures for the ten-color *in vitro* Exchange-PAINT demonstration can be found in **Supplementary Tables 3** and **4** for odd and even digits, respectively. DNA strand sequences for DNA origami structures for *in vitro* Exchange-PAINT demonstration (digits 0–3) can be found in **Supplementary Table 5**. The scaffold sequence for p8064 and M13mp18 can be found in **Supplementary Tables 6** and **7**, respectively.

DNA-PAINT imager and docking sequences as well as sequences for surface attachment via biotin are listed in **Supplementary Table 8**.

Antibody-DNA conjugates. Antibody-DNA conjugates used to specifically label proteins of interest with DNA-PAINT docking sites were preassembled in two steps. First, 3.2 µl of 1 mg/ml streptavidin (dissolved in buffer A) was reacted with 0.5 µl biotinylated DNA-PAINT docking strands at 100 µM and an additional 5.3 µl of buffer A for 30 min at room temperature (RT) while gently shaking. The solution was then incubated in a second step with 1 µl of monoclonal biotinylated antibodies at 1 mg/ml against the protein of interest for 30 min at RT. Filter columns (Amicon 100 kDa, Millipore) were used to purify the preassembled conjugates from unreacted streptavidin-oligo conjugates.

Cell immunostaining. HeLa and DLD1 cells were cultured with Eagle's minimum essential medium fortified with 10% FBS with penicillin and streptomycin and were incubated at 37 °C with 5% CO_2. At approximately 30% confluence, cells were seeded into Lab-Tek II chambered coverglass 24 h before fixation. Microtubules, mitochondria, Golgi complexes and peroxisomes were immunostained using the following procedure: washing in PBS; fixation in a mixture of 3% paraformaldehyde and 0.1% glutaraldehyde in PBS for 10 min; 3× washing with PBS; reduction with ~1 mg/ml $NaBH_4$ for 7 min; 3× washing with PBS; permeabilization with 0.25% (v/v) Triton X-100 in PBS for 10 min; 3× washing with PBS; blocking with 3% (w/v) BSA for 30 min

© 2014 Nature America, Inc. All rights reserved.

and staining overnight with the preassembled antibody-DNA conjugates against β-tubulin, COX IV, PMP70 or TGN46 (conjugates were diluted to 10 µg/ml in 5% BSA); 3× washing with PBS; postfixation in a mixture of 3% paraformaldehyde and 0.1% glutaraldehyde in PBS for 10 min; and 3× washing with PBS.

Super-resolution DNA-PAINT imaging of microtubule-like DNA origami structures. For sample preparation, a piece of coverslip (no. 1.5, 18 × 18 mm^2, ~0.17 mm thick) and a glass slide (3 × 1 $inch^2$, 1 mm thick) were sandwiched together by two strips of double-sided tape to form a flow chamber with inner volume of ~20 µl. First, 20 µl of biotin-labeled bovine albumin (1 mg/ml, dissolved in buffer A) was flown into the chamber and incubated for 2 min. The chamber was then washed using 40 µl of buffer A. 20 µl of streptavidin (0.5 mg/ml, dissolved in buffer A) was then flown through the chamber and allowed to bind for 2 min. After washing with 40 µl of buffer A and subsequently with 40 µl of buffer B, 20 µl of biotin-labeled microtubule-like DNA structures (~300 pM monomer concentration) and DNA origami drift markers (~100 pM) in buffer B were finally flown into the chamber and incubated for 5 min. The chamber was washed using 40 µl of buffer B.

The final imaging buffer solution contained 1.5 nM Cy3b-labeled imager strands in buffer B. The chamber was sealed with epoxy before subsequent imaging. The CCD readout bandwidth was set to 1 MHz at 16 bit and 5.1 pre-amp gain. No electron-multiplying (EM) gain was used. Imaging was performed using TIR illumination with an excitation intensity of 294 W/cm^2 at 561 nm.

Super-resolution Exchange-PAINT imaging of DNA nanostructures. For fluid exchange, a custom flow chamber was constructed as shown in **Supplementary Figure 6a**. A detailed preparation protocol can be found in the **Supplementary Protocol**. Prior to the functionalizing of the imaging chamber with BSA-biotin, it was rinsed with 1 M KOH for cleaning. Binding of the origami structures to the surface of the flow chamber was performed as described before. Each image acquisition step was followed with a brief ~1–2 min washing step consisting of at least three washes using 200 µl of buffer B for each. Then the next imager strand solution was introduced. The surface was monitored throughout the washing procedure to ensure complete exchange of imager solutions. Acquisition and washing steps were repeated until all ten targets were imaged. The CCD readout bandwidth was set to 3 MHz at 14 bit and 5.1 pre-amp gain. No EM gain was used. Imaging was performed using TIR illumination with an excitation intensity of 166 W/cm^2 at 561 nm (ten-color Exchange-PAINT with 3 nM Cy3b-labeled imager strands in buffer B; **Fig. 3c**,**d**) and 600 W/cm^2 at 647 nm (four-color Exchange-PAINT with 3 nM Atto 655–labeled imager strands in buffer B; **Fig. 3e**).

Super-resolution DNA-PAINT imaging of cells. All data were acquired with an EMCCD readout bandwidth of 5 MHz at 14 bit, 5.1 pre-amp gain and 255 EM gain. Imaging was performed using HILO illumination[11]. The laser power densities were 283 W/cm^2 at 647 nm in **Figure 2a** and 142 W/cm^2 at 647 nm and 19 W/cm^2 at 561 nm in **Figure 2d**.

Imaging conditions were as follows. For **Figure 2a** we used 700 pM Atto 655–labeled imager strands in buffer C. For **Figure 2d** we used 600 pM Cy3b-labeled imager strands and 1.5 nM Atto 655–labeled imager strands in buffer C.

Super-resolution Exchange-PAINT imaging of cells. A Lab-Tek II chamber was adapted for fluid exchange as shown in **Supplementary Figure 6b**. 2D images (**Fig. 4a**, **i**–**iv**) were acquired with an EMCCD readout bandwidth of 5 MHz at 14 bit, 5.1 pre-amp gain and 255 EM gain. 3D images (**Fig. 4b**–**d**) were acquired with a CCD readout bandwidth of 3 MHz at 154 bit, 5.1 pre-amp gain and no EM gain. Imaging was performed using HILO illumination in both cases. Sequential imaging was done as described for the 2D origami nanostructures, but the washing steps were performed using buffer C. The laser power densities at 647 nm were 257 W/cm^2 in **Figure 4a**, **i** and 385 W/cm^2 in **Figure 4a**, **ii**–**iv**. The laser power densities at 561 nm were 31 W/cm^2 in **Figure 4b**–**d**.

Imaging conditions were as follows. For **Figure 4a**, **i** we used 700 pM Atto 655–labeled imager strands in buffer C. For **Figure 4a**, **ii**–**iv** we used 2 nM Atto 655–labeled imager strands in buffer C. For **Figure 4b** we used 800 pM Cy3b-labeled imager strands in buffer C. For **Figure 4c**,**d** we used 2 nM Cy3b-labeled imager strands in buffer C.

3D DNA-PAINT imaging. 3D images were acquired with a cylindrical lens in the detection path (Nikon). The N-STORM analysis package for NIS Elements (Nikon) was used for data processing. Imaging was performed without additional magnification in the detection path, yielding 160-nm pixel size. 3D calibration was carried out according to the manufacturer's instructions.

Imager strand concentration determination. Optimal imager concentrations were determined empirically according to the labeling density. Generally, a high enough fluorescence off-on ratio has to be ensured in order to guarantee binding of only a single imager strand per diffraction-limited area. Additionally, a sufficient imager strand concentration (and thus sufficiently low fluorescence off-time) is necessary to ensure sufficient binding events and thereby robust detection of every docking strand during image acquisition.

Super-resolution data processing. Super-resolution DNA-PAINT images were reconstructed using spot-finding and 2D-Gaussian fitting algorithms programmed in LabVIEW[10] (**Supplementary Software**). A simplified version of this software is available for download at http://www.dna-paint.net/ or http://molecular-systems.net/software/.

Normalized cross-correlation analysis. Normalized cross-correlation coefficients were obtained by first normalizing the respective reconstructed grayscale super-resolution images and subsequently performing a cross-correlation analysis in Matlab R2013b (MathWorks).

Drift correction and channel alignment. DNA origami structures (**Supplementary Fig. 1**) were used for drift correction and as alignment markers in *in vitro* DNA-PAINT and Exchange-PAINT imaging. Drift correction was performed by tracking the position of each origami drift marker throughout the duration of each image acquisition. The trajectories of all detected drift

© 2014 Nature America, Inc. All rights reserved.
npg

doi:10.1038/nmeth.2835

markers were then averaged and used to globally correct the drift in the final super-resolution reconstruction. For channel alignment between different imaging cycles in Exchange-PAINT, these structures were used as alignment points by matching their positions in each Exchange-PAINT image.

For cellular imaging, 100-nm-diameter gold nanoparticles (Sigma-Aldrich;10 nM in buffer C, added before imaging) were used as drift and alignment markers. The gold nanoparticles adsorb nonspecifically to the glass bottom of the imaging chambers. Drift correction and alignment was performed in a fashion similar to that for the origami drift markers. Again, the apparent movement of all gold nanoparticles in a field of view was tracked throughout the image acquisition. The obtained trajectories were then averaged and used for global drift correction of the final super-resolution image. For the dual-color image of mitochondria and microtubules in **Figure 2d–f**, the gold particles were visible in both color channels. The same gold nanoparticles were also used for drift correction and realignment of the different imaging rounds in the *in situ* Exchange-PAINT experiments (**Fig. 4**).

Transmission electron microscopy (TEM) imaging. For imaging, 3.5 µl of undiluted microtubule-like DNA structures were adsorbed for 2 min onto glow-discharged, carbon-coated TEM grids. The grids were then stained for 10 s using a 2% aqueous ultrafiltrated (0.2-µm filter) uranyl formate solution containing 25 mM NaOH. Imaging was performed using a JEOL JEM-1400 operated at 80 kV.

Atomic force microscopy imaging. Imaging was performed using tapping mode on a Multimode VIII atomic force microscope (AFM) with an E-scanner (Bruker). Imaging was performed in TAE/Mg^{2+} buffer solution with DNP-S oxide-sharpened silicon nitride cantilevers and SNL sharp nitride levers (Bruker Probes) using resonance frequencies between 7 and 9 kHz of the narrow 100-µm, 0.38–N/m–force constant cantilever. After self-assembly of the origami structure, ~20 µl of TAE/Mg^{2+} buffer solution was deposited onto a freshly cleaved mica surface (Ted Pella) glued to a metal puck (Ted Pella). After 30 s the mica surface was dried using a gentle stream of N_2, and 5 µl of the origami solution was deposited onto the mica surface. After another 30 s, 30 µl of additional buffer solution was added to the sample. Imaging parameters were optimized for best image quality while the highest possible set point was maintained to minimize damage to the samples. Images were postprocessed by subtracting a first-order polynomial from each scan line. Drive amplitudes were approximately 0.11 V, integral gains were ~2 and proportional gains were ~4.

© 2014 Nature America, Inc. All rights reserved.